POLITECNICO
MILANO 1863

DIPARTIMENTO DI MECCANICA

mecc

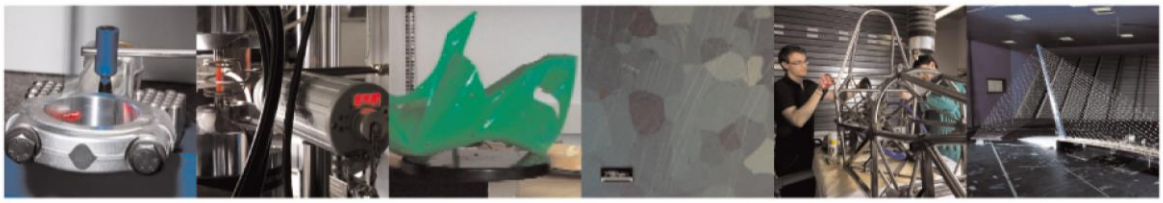

Effects of micromilled NiP mold surface topography on the optical characteristics of injection molded prismatic retroreflectors

Milan, N.; Sorgato, M.; Parenti, P.; Annoni, M.; Lucchetta, G.

This is a post-peer-review, pre-copyedit version of an article published in Precision Engineering. The final authenticated version is available online at:
http://dx.doi.org/10.1016/j.precisioneng.2019.10.006

This content is provided under CC BY-NC-ND 4.0 license

DIPARTIMENTO DI MECCANICA ■ POLITECNICO DI MILANO
via G. La Masa, 1 ■ 20156 Milano ■ EMAIL (PEC): pecmecc@cert.polimi.it
http://www.mecc.polimi.it
Rev. 0

Effects of micromilled NiP mold surface topography on the optical characteristics of injection molded prismatic retroreflectors

N. Milan[1,†], M. Sorgato[1], P. Parenti[2], M. Annoni[2], G. Lucchetta[1]

[1]*Department of Industrial Engineering, University of Padova, via Venezia 1, 35131 Padova, Italy*

[2]*Department of Mechanical Engineering, Politecnico di Milano, via La Masa 1, Milan, Italy*

[†] corresponding author, nicola.milan.5@phd.unipd.it

Effects of micromilled NiP mold surface topography on the optical characteristics of injection molded prismatic retroreflectors

Nicola Milan, Marco Sorgato, Paolo Parenti, Massimiliano Annoni, Giovanni Lucchetta

Abstract

Automotive lighting applications require mold micro-features with increasingly better surface finishing, especially for optical lenses and retroreflectors. In this work innovative micromilling experiments were conducted on electroless-plated nickel phosphorous (NiP) surfaces to fabricate a mold for prismatic retroreflectors. Cutting parameters effects on surface topography of mold micro-features were experimentally characterized and optimized, monitoring moreover the cutting forces generated by NiP micromilling. Furthermore, the mold surface topography was replicated on polycarbonate injection molded retroreflectors and its effects on their optical performance was characterized by means of a dedicated spectrophotometric technique. The obtained results show that micromilling of electroless-plated NiP can substitute polishing in the fabrication of high surface finish mold micro-features.

Keywords: micro machining, topography, replication, NiP

Acknowledgements

The authors gratefully acknowledge Brenta Group Spa for its technical and commercial support.

Abbreviations

BEM Ball End Mill

CER Cutting Edge Radius

FEM Flat End Mill

MQL Minimum Quantity Lubrification

NiP Nickel-Phosphorus

PBE Pin Bundling Electroforming

RR Retroreflector

a_e Radial depth of cut

a_p Axial depth of cut

f_z Feed per tooth

V_c Cutting speed

Roughness parameters

Sa Arithmetic mean height

Sq Root mean square height

Sdr Developed interfacial area ratio

Str Texture aspect ratio

1. Introduction

Nowadays, automotive lighting market increasingly required three-dimensional mold micro features, such as micro grooves, micro lenses and micro prisms with polished surfaces. In particular, retroreflectors (RRs) are optical devices made of transparent plastics and normally utilized in automotive lighting devices to return incoming light and to make the vehicle visible while driving in low light conditions. Their functionality is based on the inverted corner cube geometry, a hexagonal-shaped optical structure delimited by three mutually perpendicular square faces that are lapped to optical surface quality [1]. This particular geometry enables the incident light to be retroreflected after three internal consecutive reflections, according to the optical principle called total internal reflection. Retroreflective performance is typically quantified as the ratio between the retroreflected and incident light intensity [2].

Generally, the mold surfaces are finished by hand polishing technique occupying dedicated human operators for several days [3]. However, this finishing technology couldn't be applied to micro-optical devices without damaging their shapes. Thus, their final surface finish is given by the process used to create them.

High quality RRs are conventionally manufactured using the pin-bundling-electroforming (PBE) technique, schematically described in Figure 1 (a). PBE can be divided into a sequence of steps that begins with the lapping of the forming end of pins having a hexagonal cross section. Each of the three mutually perpendicular faces is lapped until its surface roughness reaches the low nanometric range (Sa ~ 10 nm). The pins are then bundled together in such a way that their ends match the final 3D shape of the taillight to be molded. They are then used as a master in an

electroforming bath to generate a thick and hard nickel-based layer, which is then used as a mold insert in the final injection molding step for mass-scale replication.

In a recent study Milliken et al. report that the average areal roughness of the retroreflective facets of a RR manufactured by means of the PBE technique is 9.2 nm while their average waviness, *Wa*, is 29.9 nm [4]. However, even though analytical correlations between surface roughness, amount of reflectance (and scatter) and the incident light characteristics have been proposed [5], the effect of surface roughness and waviness on retroreflection are still not completely understood.

Since the primary purpose of the automotive retroreflectors is to make the preceding vehicle as visible as possible, a certain amount of light scatter might be beneficial [4]. Thanks to their good technical properties, such as low water absorption, high transparency and reduced internal stresses, Polymethylmethacrylate (PMMA), Polycarbonate (PC) and Cyclin Olefin Copolymer (COC) are widely uses for injection molded optical micro features [6,7].

The PBE manufacturing process is very time consuming (7–12 weeks depending on the design complexity and overall size of the RR) and has a typical cost of approximately $400 USD/cm^2 for a generic corner cube-based retroreflective area [4]. Another major disadvantage of PBE of RRs on non-planar surfaces is related to the presence of the pocket-like features shown in Fig. 1b, which significantly reduce the optical performance of RRs by acting as light traps [2]. Moreover, these manufacturing artifacts generate undercuts onto the electroformed mold insert that in turn require higher demolding forces for the ejection of the molded parts. These undercuts are also prone to damage while also being difficult to repair [8].

1.1. Recent developments

In the next years, newer trends in automotive styling and lighting will increasingly require freeform RR designs.

Freeform surfaces introduce new challenges both in optical manufacturing and in measurement. Recent optical design leads to uneven surface structure and more complex micro feature. Ultraprecise micro scale fabrication technologies are natural candidate to overcome PBE drawbacks [2, 5, 8, 9]. Indeed, traditional machining technology, such as turning and milling, are widely used in mold maker industry thanks their low operating cost (about 60€/h), low lead time and possibility to obtain freeform geometries. In particular, ultra-precision turning of electroless-plated nickel phosphorous (NiP) surfaces by means of single crystal diamond tools has been successfully employed to fabricate molds for lenses achieving roughness values (*Sa*) under 10 nm, especially when the phosphorus content exceeds 10% [10]. In fact, this element increases the ductility of nickel, improving its machinability and surface quality by reducing the tool wear.

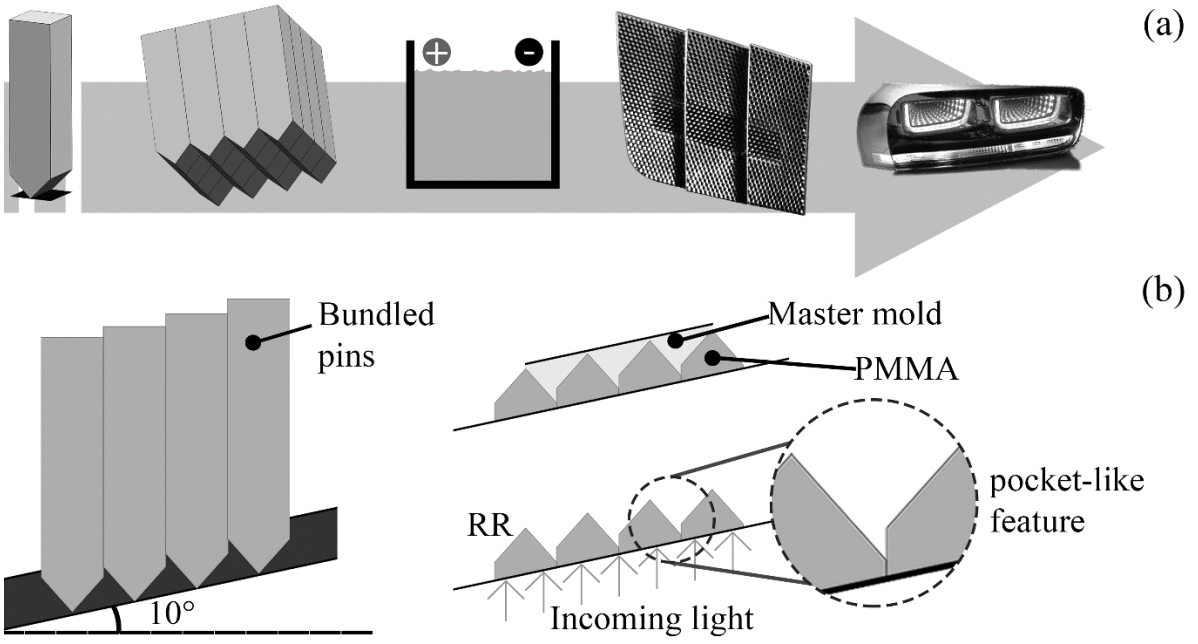

Fig. 1. RR manufacturing by (a) pin-bundling-electroforming and (b) pocket-like features generation on non-planar surfaces.

Recent microgrooving experiments on NiP by means of a V-shaped diamond tools show how it is possible to obtain micro features with a high surface quality [11, 12]. Roeder et al. obtained a micro lens arrays with a single-flute diamond milling tool, exploiting a vertical immersion of the tool [13]. However, micromilling of NiP-coated molds for complex 3D optical parts has not been attempted yet. Consequently, no previous data about NiP cutting forces, cutting parameters and tool selection influence are reported in scientific literature. Therefore, the main objective of the present study is to introduce micromilling of electroless-plated NiP as a viable manufacturing option for the fabrication of molds for RRs, as an alternative to the ineffective conventional PBE technology. Cutting parameters effects on mold surface topography were experimentally characterized and optimized, monitoring at the same time the cutting forces. Moreover, the mold

surface texture was replicated by injection molding on polycarbonate RRs and its effects on their retroreflective performance was characterized by means of a special designed spectrophotometric procedure.

2. Materials and Methods

2.1. Retroreflector design and mold inserts coating

A mold insert characterized by four identical rectangular-base prisms was designed as depicted in Fig. 2b. Each prism has four tilted surfaces and three of them are tilted at different angles to assess the achievable surface finishing quality with the adopted 3-axis machining. Since micromilling was never attempted on amorphous NiP coatings, no previous knowledge was available for suggesting the optimal cutting parameters for this material. For these reasons, a second flat insert, shown in Fig. 2a, was designed to carry out simple slotting tests for the optimization of the cutting conditions on the NiP coating, using a micro dynamometer for the cutting force measurement. In fact, this type of test is widely used because it allows separate the influence on the material machinability of the cutting parameters from the CAM toolpath [14]. The optimal cutting parameters values obtained by studying this insert were then used to machine the prismatic mold insert.

The substrate material is an AISI H13 steel (46-48 HRC), which is widely adopted in the mold industry. A material allowance of 250 μm was prescribed considering the thickness of the coating and a nominal machining allowance for the NiP milling. The milled inserts were then coated respectively with a 500 μm (flat insert, Fig. 2a) and 250 μm (prismatic mold insert, Fig.

2b) layer of amorphous NiP, having a phosphorous content of 10%. The measured coating hardness was about 49-55 HRC.

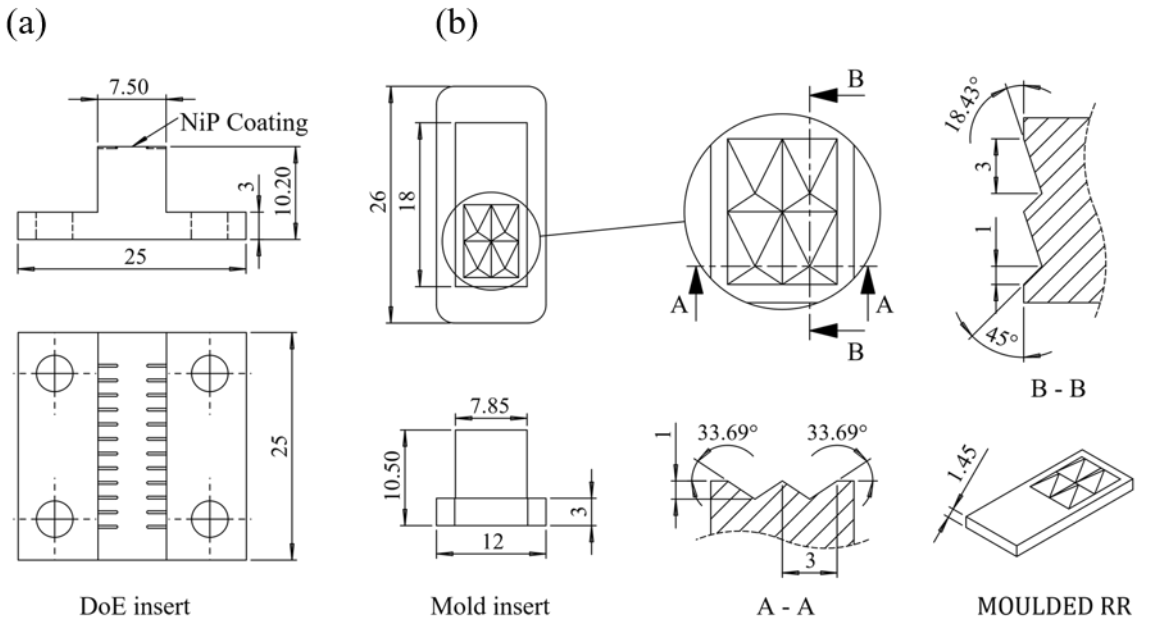

Fig. 2. Design of (a) the flat insert for the cutting tests and (b) of the mold insert for the prismatic geometry

2.2. Cutting tests on NiP coating

To ensure the sufficient level of accuracy and repeatability, the experiments were carried out on a micromilling center (Kugler, Micromaster 5X, Fig. 3a) with a maximum spindle speed of 60 krpm with the adopted electrospindle. The optimization experiments consisted in slotting operations carried out on the flat insert with two types of Ø 0.3 mm flat-end mills (FEM, as referred in Parenti et al. [15]): coated (Seco, Mini 905003 Mega T, coating thickness 2µm) and uncoated ones (Zecha, 481.030). The two mill types allowed testing different tool sharpness levels, i.e. different cutting edge radii (CER), on the cutting performance and surface finish. Recent advances in machining modeling allowed to predict the machinability of a material by

means of cutting force measurement [16-17]. Cutting forces were acquired by means of a micro dynamometer (Kistler, 9317B, Threshold <0.01N, Fig.3b), three amplifiers (Kistler, 5015 A) and an acquisition board (National Instrument, 9234) at a sample rate of 51.2 kHz. The RMS of resultant cutting forces, was elaborated after compensating the pure dynamic behavior of the dynamometer. A 3D optical microscope (Alicona, Infinite Focus G4) was used to measure the CER of the cutting tools that resulted approximately 1.5 µm for the uncoated and 9 µm for the coated tools.

The cutting optimization was carried out according to a full-factorial design with two factors, i.e. cutting speed, V_c, and feed per tooth, f_z, varied on three levels, leading to 9 experimental runs for each milling tool. The levels for each factor, which are reported in Table 1, were selected based on preliminary cutting experiments that considered the geometry and CER values of the tools. A series of 2-mm-long slots were milled in full slotting (i.e. a_e = 0.3 mm) whilst the axial depth of cut, a_p, was set to 20 µm, which is typical for finishing passes. Cooling and lubrication were performed with a MQL system as suggested by scientific literature [10, 12, 13]. The response variable to minimize was the Surface finish, evaluated through the areal roughness parameter *Sa*.

In order to evaluate the tool wear, the central point of the experimental plan was additionally replicated twice, i.e. before and after the plan. All the experiments were replicated 3 times for a total of 33 tests per type of mill. In order to test the homogeneity of the NiP coating characteristics along the whole layer thickness, the three replications were carried out, using new tool units, on the same insert after machining the previous slot series by face milling (a_p = 100 µm) with a Ø 3 mm flat-end mill (Zecha, 596.040.0300).

Table 1: Factors levels for the optimization plan with flat-end mills

Level	Uncoated mill		Coated mill	
	V_c [m/min]	f_z [µm]	V_c [m/min]	f_z [µm]
-1	14	0.5	14	5
0	21	1.5	21	7
1	28	2.5	28	10

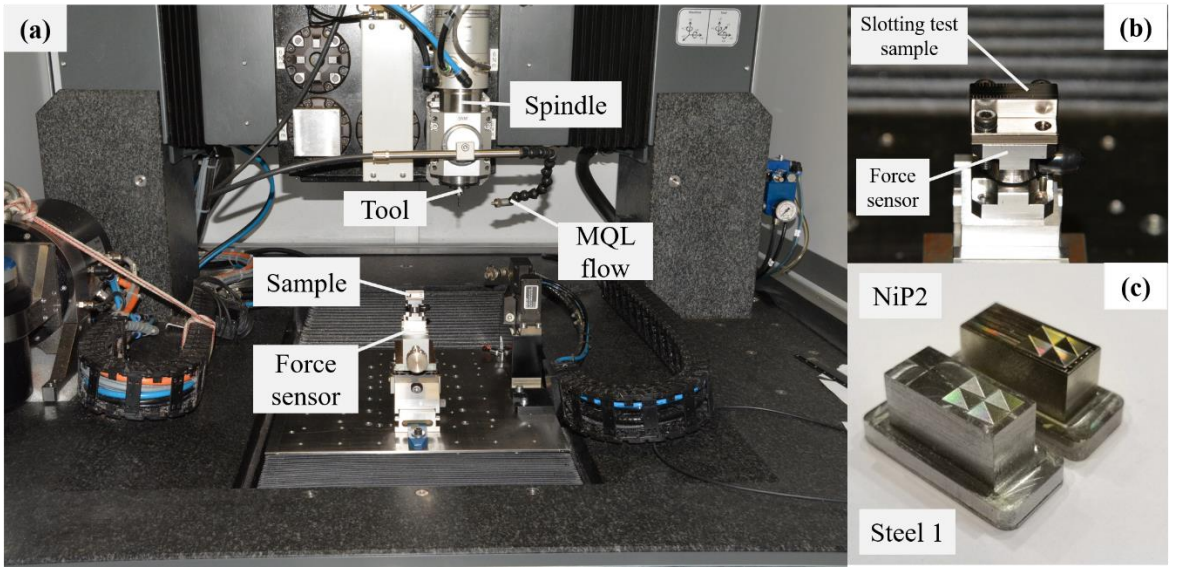

Fig. 3. (a) Setup used in the whole milling experimental campaign, in particular for (b) the force signal acquisition and for machine (c) the retroreflector mold inserts.

2.3. Micromilling and injection molding of the prismatic geometry

On the basis of the optimization experiments explained in the previous paragraph, which declared the use of uncoated tools as the most promising for surface finishing (as reported in paragraph 3.1) , micromilling of the NiP-coated RR prismatic geometry was carried out with an uncoated Ø 0.3 mm ball-end milling tool (Zecha, 590.030.0030). As typical in mold manufacturing, a ball-end tool geometry (BEM) was adopted for the prism, instead of a FEM, because this tool geometry is the most suitable for achieving smooth inclined surfaces, especially when 3-axis machining cycles are adopted. When machining complex mold surfaces, in facts, the final achievable roughness is also strongly affected by kinematic aspects related with the adopted CAM strategy and the scallops formed by tools during the multiple overlapped passes on the mold surface.

The selection of the BEM cutting parameters was driven by the surface finish optimal values obtained from the FEM tools optimization cutting plan explained in the previous paragraph, with the idea that these two tool types share most of the basic tool-material interaction phenomena that lead the cutting performance, as the surface generation. In particular, for the BEM the adopted parameters were V_c = 20 m/min and f_z = 2 µm, considering a compromise between surface finishing and machining time. Initially the RR prismatic geometry was rough milled on the steel insert, Fig 4a, with a Ø 0.6 mm ball-end tool (Zecha 590.030.006BCR).

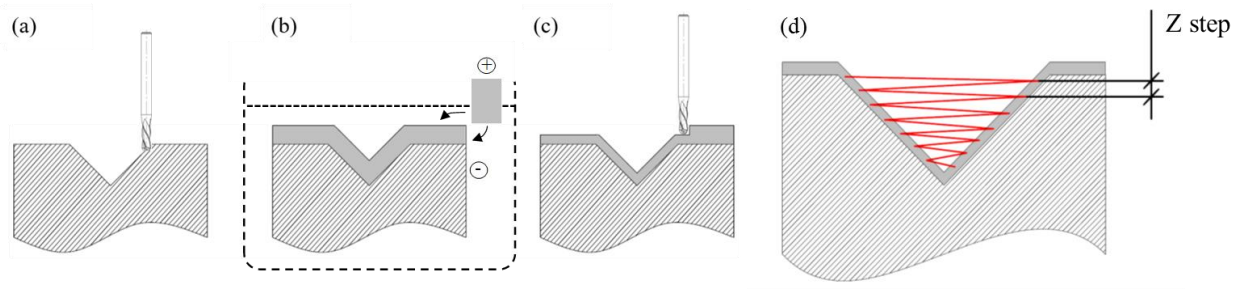

Fig.4. Scheme of the RR manufacturing with (a) prism fabrication using a traditional roughing process, (b) NiP coating deposition, (c) finishing passes and (d) CAM spiral toolpath.

Afterwards, a 250 µm NiP layer was applied on the top surface of the mold insert coated the whole prisms, as shown in Fig. 4b. Eventually, 40 µm of the NiP layer were removed using a spiral CAM toolpath in two passes with a new ball end tool for each prism (Fig. 4c).

In order to vary the surface finish and to investigate its correlation with the RR optical performance, two NiP-coated mold inserts, NiP 1 and NiP 2, were machined with a Z step of 10 µm and 4 µm, respectively (Fig. 4d). Furthermore, to generate a reference for comparison, as shown in Fig. 3c, two uncoated prismatic mold inserts in AISI H13 steel, called Steel 1 and Steel 2, were machined using two coated Ø 0.3 mm ball-end milling tools (Hitachi EPDBE_2003-0.5-ATH and Hitachi CBN-EHB-2003) with different CER (4 µm and 9 µm, respectively). These inserts were machined using a Z step of 4 µm and cutting parameters optimized in previous experiments: V_c = 22 m/min and f_z = 4 µm for Steel 1; V_c = 20 m/min and f_z = 9 µm for Steel 2. All milling tools were inspected prior and after cutting by means of a SEM in order to ensure the integrity. All the used tools guaranteed extremely low values of static tool run-out (less than 1 µm on the shank as measured on board by means of a comparator device). The use of an ultra-precise and ultra-repeatable fixturing (System3R MacroNano) simplified the transfer of the

samples under the 3D microscopes for the periodic workpiece inspections that were carried out during all the cutting tests. The whole milling tools used in this work are summarized in table 2. A polycarbonate that is widely used in taillight applications (Covestro, Apec 1695) was chosen to mold the plastic retroreflectors by means of a micro injection molding machine (Wittmann-Battenfeld, MicroPower 15) and a specially designed mold, illustrated in Fig. 5a. The injection molding parameters were set as suggested by the material supplier in order to maximize the replication of the insert topography. In particular, high range values for both melt and mold temperature were selected: T_{melt} = 320°C and T_{mold} = 100°C [18].

Table 2: Summary of the milling tools used in this work

Workpiece	Tool	Diameter [mm]	Geometry	Coated	Cutting Configuration
NiP DOE Sample	Zecha, 481.030	0.3	FEM	No	Full radial immersion
NiP DOE Sample	Seco, Mini 905003 Mega T	0.3	FEM	Yes	Full radial immersion
NiP DOE Sample	Zecha, 596.040.0300	3	FEM	No	Face milling
NiP mold insert	Zecha, 590.030.0030	0.3	BEM	No	RR finishing
Steel mold insert	Hitachi, EPDBE_2003-0.5-ATH	0.3	BEM	Yes	RR finishing
Steel mold insert	Hitachi, CBN-EHB-2003	0.3	BEM	Yes	RR finishing

2.4. Topography and optical characterization

Limited depth of the milled features allowed direct topography measurements on the samples, avoiding the need of using indirect methods [19]. A confocal microscope (Sensofar, PLU Neox)

with 20 X and 100 X objectives was then used for the surface characterization of both the machined mold inserts and the molded RRs.

Stitched areas of 150 x 150 µm were acquired, then shape removal was applied and the parameters *Sa*, *Sq*, *Sdr*, *Str* and *Wa* were calculated according to ISO 25178 and ISO 4288 standards [19, 20]. The final roughness of the prisms was characterized considering a weighted average based on the surface area of every prism face.

The optical performance of the molded retroreflectors was evaluated with an innovative dedicated experiment in order to understand the influence of the molded surface topography on the optical performance. The experimental campaign was carried out by means of a spectrophotometer (Jasco, V-570) equipped with an integrating sphere, as shown in Figure 5b. The ratio between the retroreflected and incident light intensity was measured, using an 8x9 mm light beam (wavelength 300 – 850 nm) incidenting the prisms in the concave surfaces

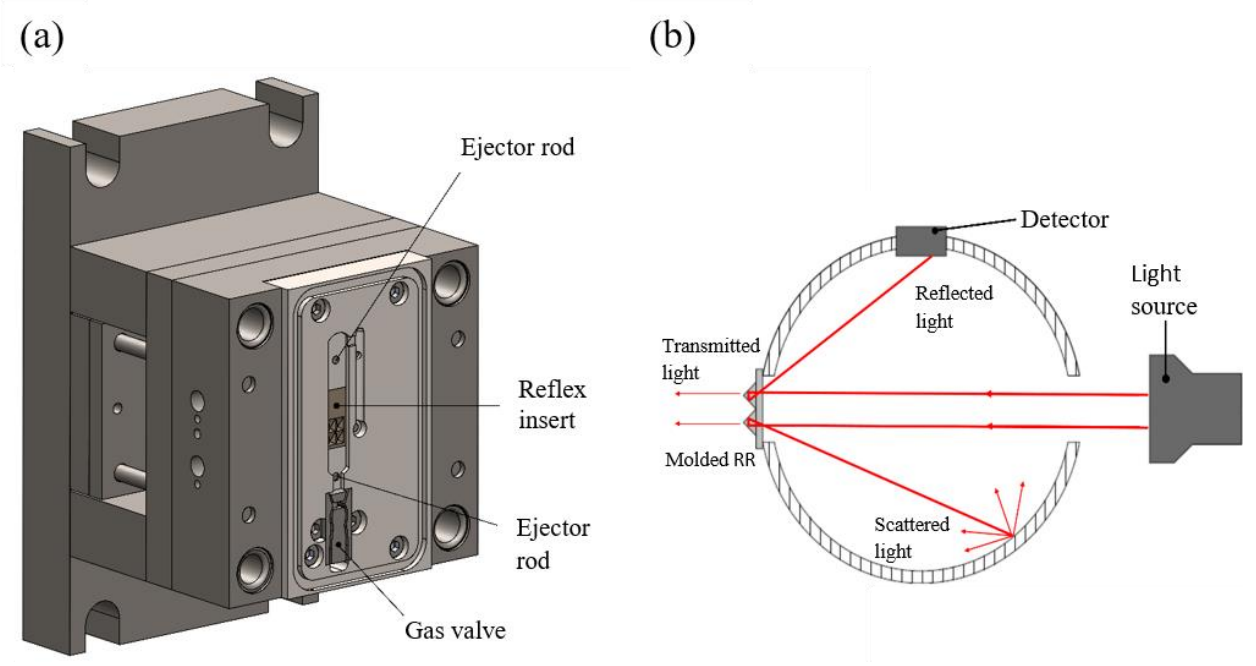

Fig.5. Representation of (a) the mold designed and used in this work and (b) the scheme of the optical characterization

with an angle of 5°. The correlation between the surface finish and the retroreflective performance was evaluated at a wavelength of 550 nm, in the middle of the visible light range.

3. Results and discussion

3.1. Cutting test results

3.1.1. Cutting forces

The machinability of the coating material toward the achievement of extreme surface finish can be assessed by analyzing the micromilling forces measured during the cutting of the flat insert. Extreme low values of cutting forces were measured and an overall limited tool wear was observed despite the high hardness of the coating material. No tool breakage occurred indicating a suitable selection of the cutting condition to test. Frequency analysis of the signals confirmed that regular cuttings were obtained without the presence of unwanted vibrations. Cutting forces in X and Y direction assumed the typical pseudo-period shape and seemed not too much affected by the workpiece entry and exit transient stages, indicating relatively limited cutting tool deflections. Vertical force in Z-direction, showed more random behaviors but always limited values, indicating good chip evacuation properties and clearance design of the end mills. At the same time, the adoption of different feed per tooth, f_z, for the two sets of tools (uncoated and coated) caused extremely different force values in the testing. The worst conditions for the uncoated tools resulted the highest cutting speed (V_c =28 m/min) and feed per tooth (f_z =2.5 µm)

that produced a RMS of resultant cutting force equal to F= 0.3159 N, Figure 6(a). Minimum force values were achieved at the lowest cutting speed and feed per tooth (f_z =0.5 µm), Figure 6(a). On the opposite, the coated tools reached a RMS equal to F=1.189 N for the biggest feed per tooth adopted (f_z =10 µm) and the intermediate value of cutting speed (V_c =21 m/min).

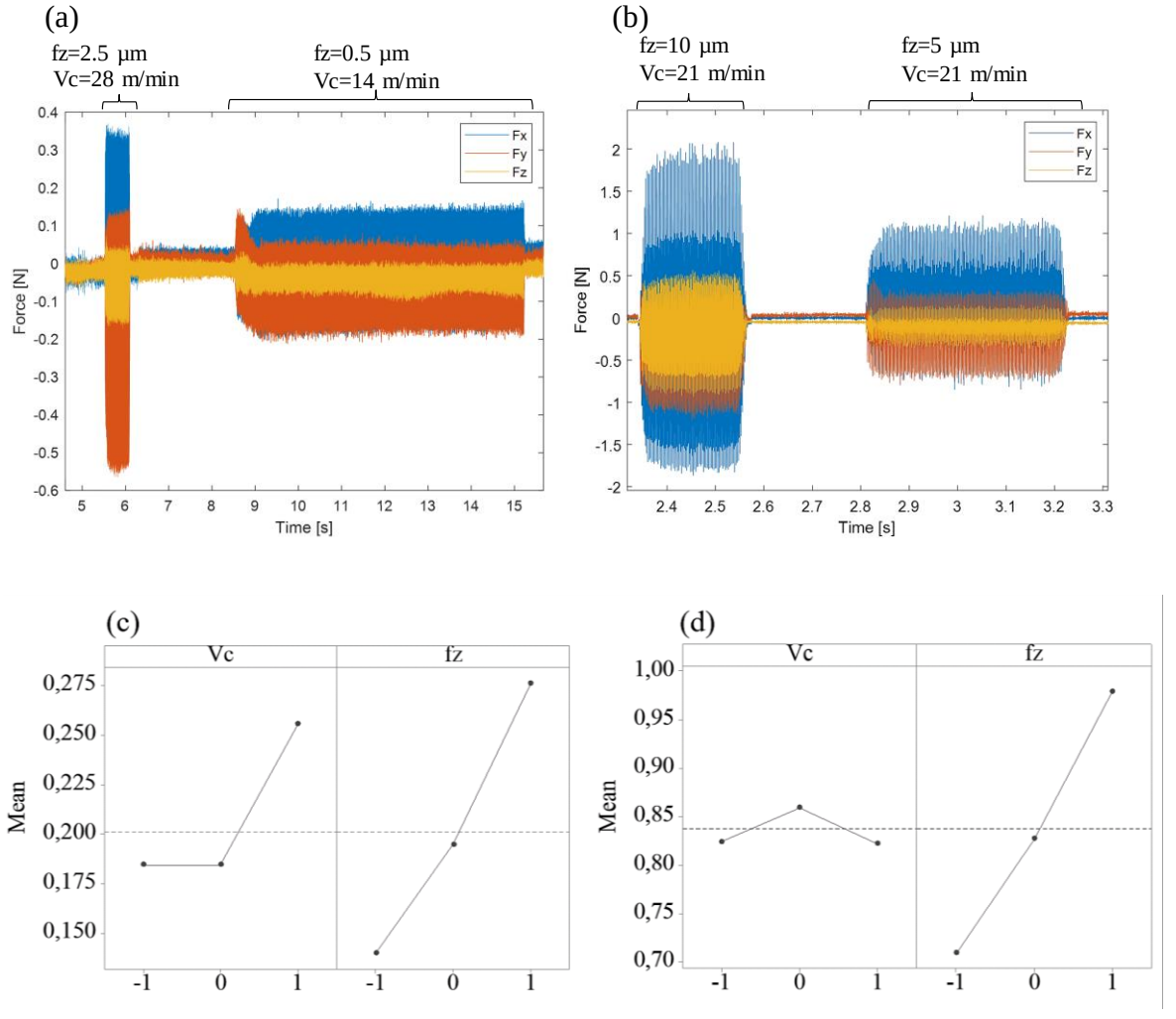

Fig. 6. (a-b) RMS of resultant cutting force on time domain plot: (a) uncoated tool, (b) coated tool; (c-d) related Main Effect plot: (c) uncoated tool, (d) coated tool;

The Main Effect plots in Figure 6c and 6d, describe the change of the average values of the resultant cutting force for a change of the cutting parameters. Despite the limited extension of the experimental campaign performed, it is possible to appreciate the effect of the feed per tooth value, which increase parabolically the force values. In general, the cutting speed played a minor role on the forces and its effect was irrelevant on the coated tools forces. However, the cutting speed contribute to the forces increased on the uncoated tool, causing a relevant increase of the forces in a quite unexpectable way.

3.1.2. Surface topography

The ANOVA performed on the cutting optimization results on NiP coating showed that the influence of cutting speed and feed per tooth on surface roughness (*Sa*) is significant for both coated and uncoated milling tools. As shown in Figure 8, f_z has a larger influence on *Sa*. In general, the topography characterization (Fig.7) showed that uncoated tool achieved better surface quality with the lowest *Sa* of 15 nm and a RMS resultant cutting force of 0.07 N. The coated tools, instead, were able to reach a *Sa* of 63 nm with a RMS resultant cutting force of 0.37 N, confirming the influence of the tool CER on the force and surface topography generation.

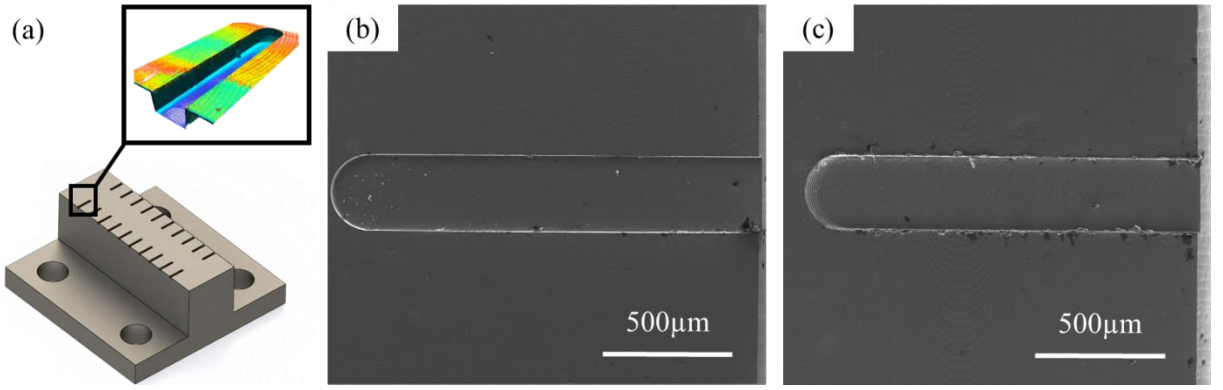

Fig. 7. Topography characterization of the slots by means of (a) optical profiler and SEM for the DOE central point of (b) uncoated and (c) coated tool;

As reported in Figure 8a, 8c, both the uncoated and coated mills showed a positive trend on the f_z/*Sa* plot, as expected from the micromilling process and cutting kinematics. However, the influence of f_z on *Sa* is higher for coated tools. This is likely due to the higher forces that these tools generate with the adopted larger feed values. In fact, higher cutting forces acting on similar tool bulk geometries (as the coated and uncoated tools have) lead to higher tool deflections and vibrations that may have affected the surface generation. Conversely, V_c had an unexpected, although minor, influence on surface roughness. *Sa* has a marked and inverse dependence on V_c with coated tools whilst it shows a less significant and direct relation with uncoated ones, as reported in Figure 8b, 8d. This is likely due to the higher average force levels exhibited by the coated tools and to the impact that cutting speed has on heat generation and on consequent material softening, especially when cutting hard materials. This agrees with the observed force reduction and surface finishing improvements for the coated tools for higher values of *Vc*. The fact that increasing *Vc* gave worse finishing with the uncoated tools, together with the fact that

these tools increased the generated forces when higher cutting speeds were adopted, remains unclear. These facts, surely coupled by the cutting mechanisms, require further investigations.

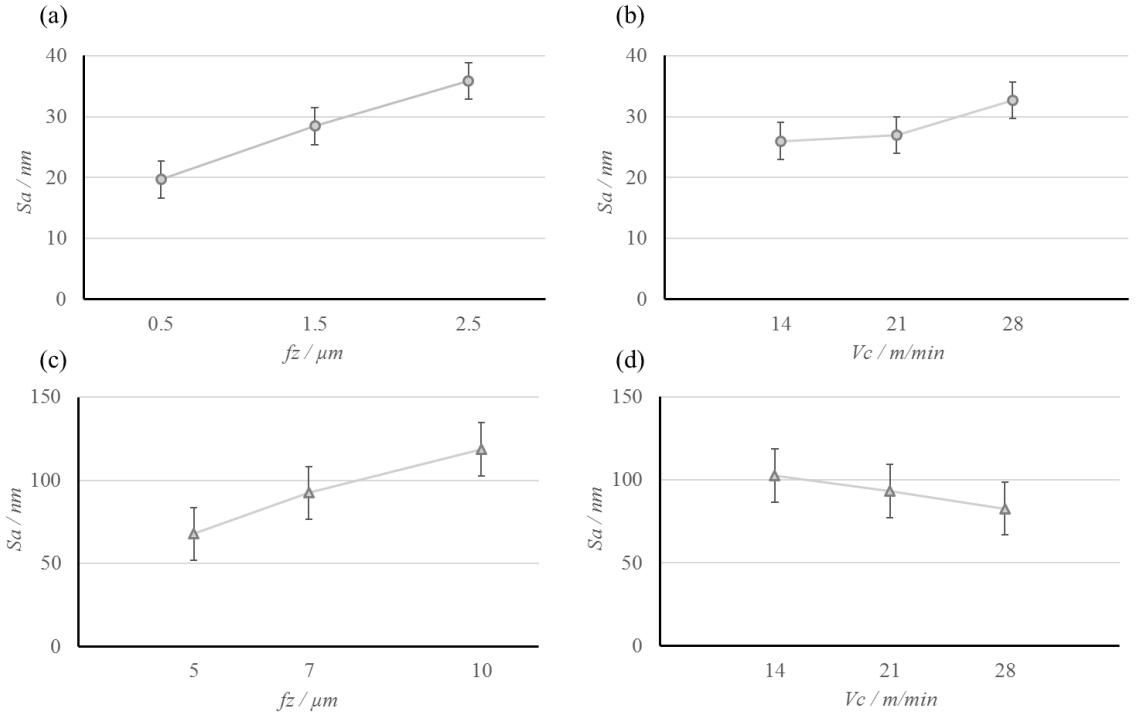

Fig. 8. Main effects of (a,c) feed per tooth and (b,d) cutting speed on surface roughness (Sa) for (a,b) uncoated and (c,d) coated milling tools. Max St. Dev. is 3 nm for the uncoated tools and 16 nm for the coated ones

The showed link between cutting parameters and surface finish can be further discussed in terms of relationship between the achievable finish and the generated cutting forces. In particular, the *Sa* roughness values achieved with the uncoated tools were distinctly linked to the generated resultant cutting force values, see Figure 9, where the lower the forces, the better the finish.

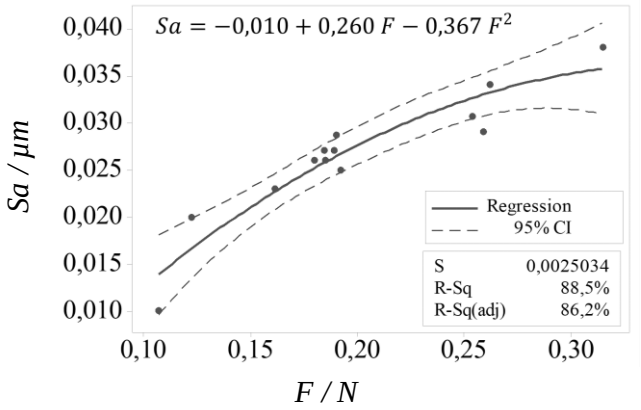

Fig. 9. Regression between RMS value of resultant cutting force and achievable surface finish *Sa* (uncoated tools)

This empirical trend, clearly showed by the uncoated tools, links the cutting mechanisms with the texture generation and can help in finding the optimal setup conditions in presence of finish requirements on the NiP coated molds. However, the coated tools did not show such as clear behavior most likely due to the bigger forces generated by the adoption of larger feed per tooth values, as required by the less sharp tools. An increase of forces has a direct effect on tool static/dynamic tool deflections that has a strong impact on cutting mechanism and therefore on surface texture generation.

As regards the tool wear and coating inhomogeneity, the ANOVA performed on both the results from the three replications of the central point and the replications of the whole experimental plan at different depth of the coating layer, showed that the effects of these two phenomena were negligible.

The cutting optimization results indicated that the uncoated tool was the best option to mill the NiP-coated RR prismatic geometry. In particular, V_c = 20 m/min and f_z = 2 µm were chosen for

the mold insert machining (with the ball-end tools) as a compromise between surface finishing and machining time.

3.2. Mold insert and molded RR surface topography

The results of the surface characterization of the NiP-coated mold inserts and their molded RRs are summarized in Table 3 for each tilt angle of the prism faces. They show that this novel micromilling approach was able to achieve an average *Sa* of 56 nm and an average *Wa* of 37 nm with a Z step of 4 µm (NiP 2). The comparison of these values with the ones of the PBE technology (*Sa* = 9.2 nm, *Wa* = 29.9 nm [4]) shows that the proposed approach still needs to be improved but only in terms of surface roughness.

Table 3 Mean and standard deviation (in brackets) values of surface roughness and waviness for the NiP-coated molds and their molded RRs

Tilt angle	Mold insert		Molded RR	
	***Sa* [nm]**	***Wa* [nm]**	***Sa* [nm]**	***Wa* [nm]**
		NiP 1		
45°	233 (19)	37 (3)	203 (10)	28 (3)
33.7°	86 (8)	47 (6)	94 (2)	28 (2)
18.4°	93 (9)	32 (2)	105 (7)	29 (3)
Avg.	137	39	135	28
		NiP 2		
45°	67 (5)	27 (3)	72 (6)	27 (1)
33.7°	50 (3)	47 (5)	54 (2)	23 (1)
18.4°	59 (7)	38 (4)	49 (1)	20 (2)
Avg.	56	37	61	23

The prisms of the NiP 1 insert had an average *Sa* of 137 nm due to a higher Z step of 10 µm. Similar values of roughness for the polycarbonate RRs show that the selected injection molding parameters allowed a good replication of the mold surface topography.

The results of the surface characterization of the steel mold inserts and their relevant molded RRs are summarized in Table 4 and in Figure 10. Comparing them with the ones obtained for the NiP-coated mold inserts, it is evident the effect of the NiP coating on improving the mold machinability and surface quality. In fact, the NiP-coated topographies present well defined cutting marks, without relevant appearance of ploughing, as shown in Figure 11.

Table 4. Surface roughness of the steel mold inserts and their molded RRs

Tilt angle	**Steel 1 *Sa* [nm]**				**Steel 2 *Sa* [nm]**			
	Mold insert		**Molded RR**		**Mold insert**		**Molded RR**	
	Avg.	**St. Dev.**	**Avg.**	**St. Dev.**	**Avg.**	**St. Dev.**	**Avg.**	**St. Dev.**
45°	146	5	169	14	232	1	247	17
33.7°	116	12	108	14	167	3	151	10
18.4°	85	12	89	4	110	9	101	8
Avg.	122		126		180		176	

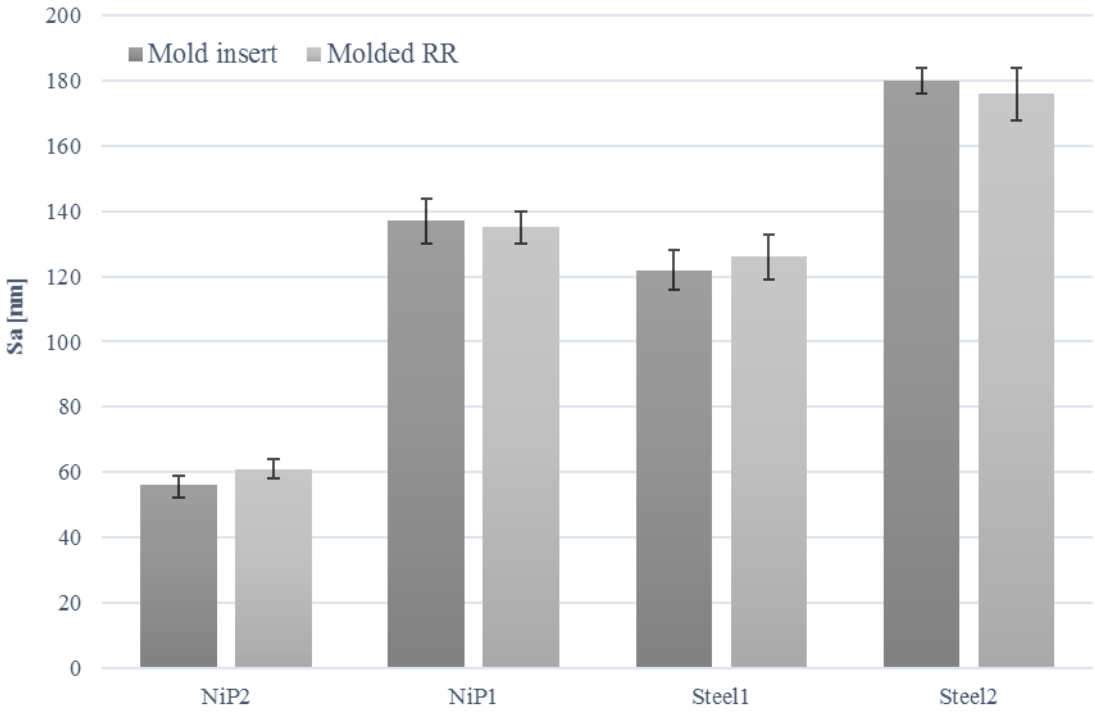

Fig. 10. Roughness Parameter Sa for the Mold Insert and the Molded RR

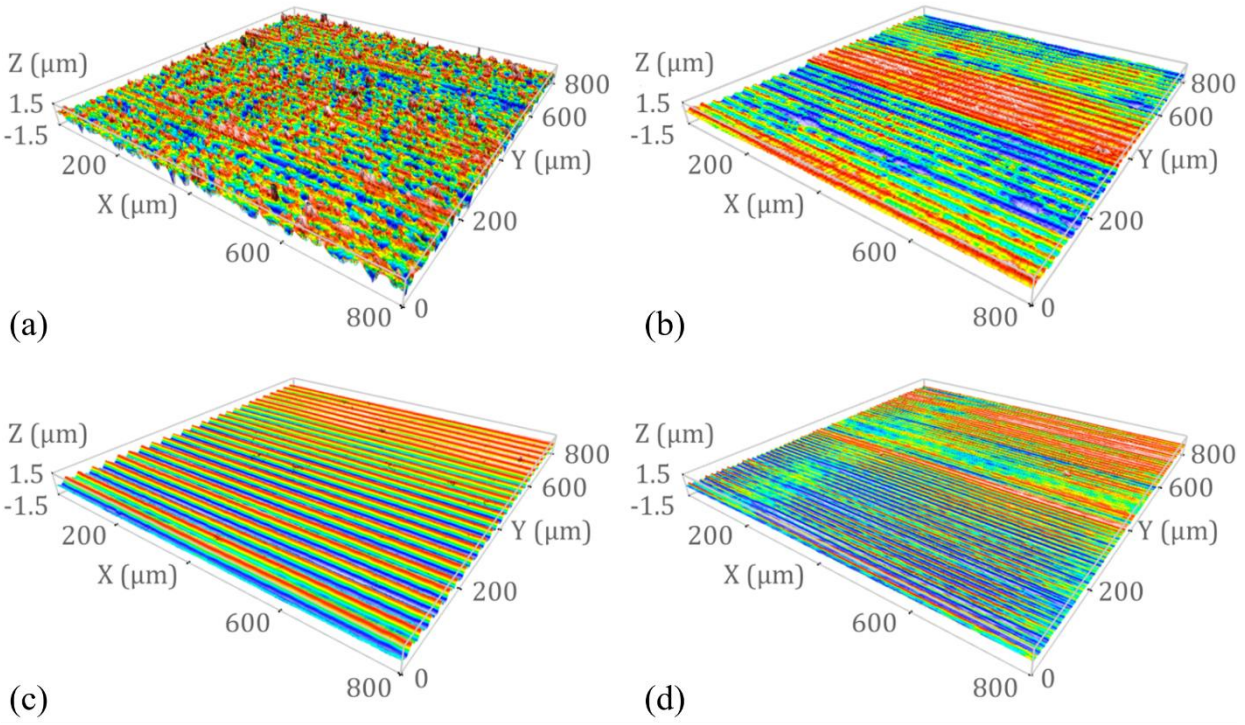

Fig. 11. Surface topography of the 18.4° tilted faces on (a) Steel 2, (b) Steel 1, (c) NiP 1 and (d) NiP 2 mold inserts

In other to further investigate the different textures obtained on the molded RRs, the parameters *Sq*, *Str* and *Sdr* were calculated. Their average values are reported in Table 5. The texture aspect ratio parameter, *Str*, which characterizes the surface isotropy [22], shows that machining of NiP produced a more anisotropic surface with a dominant texture direction, as shown in Fig. 10. The complexity of the surface, represented by the *Sdr* parameter, revealed that the NiP 1, the NiP 2 and the Steel 1 had a flatter surface than the Steel 2. The *Sq* parameter in general followed the *Sa* trend with NiP 1 and Steel 1 showing a similar value.

Table 5. Surface texture parameters for the RRs molded with NiP-coated and steel inserts

Parameter	NiP 1	Nip 2	Steel 1	Steel 2
Sq [nm]	151	72	155	213
Sdr [%]	0.18	0.18	0.18	0.35
Str	0.009	0.01	0.081	0.048

3.3. Optical characterization

The dedicated test design allowed understand the influence of the surface finish on the optical behavior. Both the *Sa* and *Sq* average values for the molded polycarbonate RRs were related to their retroreflective performance at a wavelength of 550 nm, i.e. in the middle of the visible light range, finding a linear correlation with the surface finish, as shown in Figure 12. In particular, NiP 2 has a retroreflective performance higher than Steel 1, NiP 1 and Steel 2 respectively by 10%, 13% and 21%. The lower *Sq* the higher the reflection and scattering of light. This is due to the fact that *Sq* is directly related to the surface energy and the way the surface scatters the light [22]. A further improvement of surface finishing will therefore increase the retroreflective performance of RRs manufactured by micromilled NiP-coated molds.

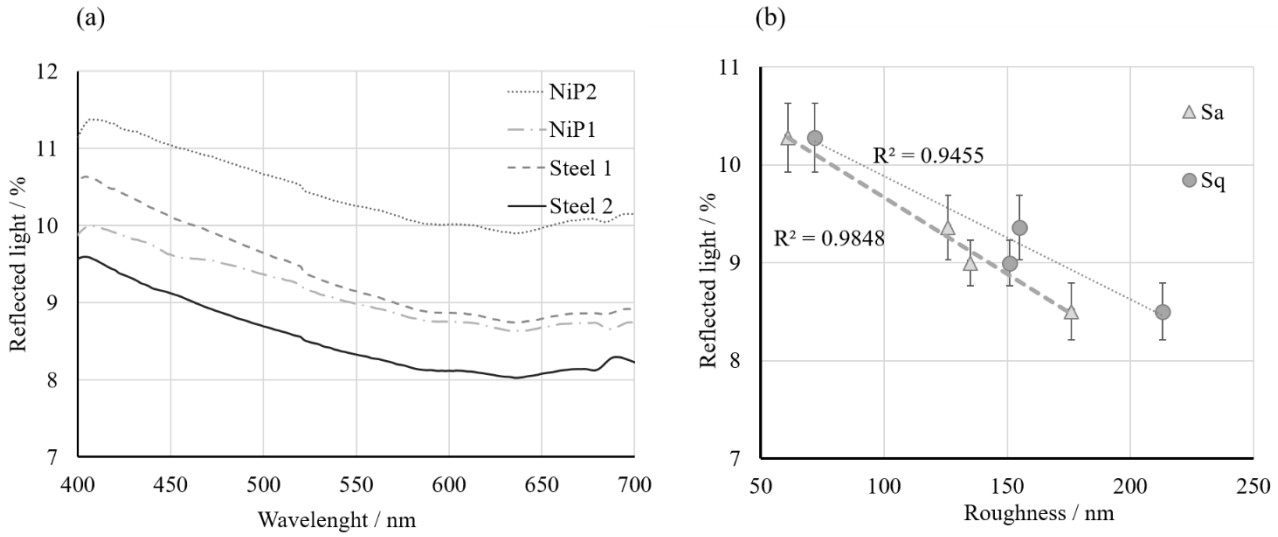

Fig. 12. Results of the optical characterization in terms of (a) reflected light for the different mold inserts and (b) correlation between retroreflective performance and surface roughness of the molded RR

4. Conclusion

The main objective of the current study was to introduce micromilling of electroless-plated NiP as a valuable manufacturing option for the fabrication of molds for RRs and as an alternative to the ineffective conventional PBE technology.

The results obtained in this work could be summarized as follow.

- The NiP coating presents a good machinability with negligible tool wear, proving to be suitable for achieving polished surface finishing by means of ultra-precise micromilling with a best result of 15nm in terms of *Sa*.
- The cutting forces were in line monitored by means of a microdynamometer, showing extreme low values, in particular for uncoated FEM. Moreover, an empirical correlation between the surface finish and the cutting forces were found.

- The Ø 0.3mm FEM uncoated achieved a surface finishing of *Sa* 15 nm in a full slot test with V_c = 21m/min , f_z = 0.5 µm/t and a_p =20µm
- A RR insert mold was micro machined with a Ø 0.3mm BEM uncoated, reaching an average roughness, in terms of *Sa* parameter, of 56 nm.
- Both the mold insert and the molded component topographies were characterized in terms of surface roughness and waviness, verifying the good replication obtained by means of microinjection molding.
- The optical characterization of the molded RRs, carried out by means of a dedicated spectrophotometric technique, has revealed a linear correlation between the reflected light and the surface roughness parameters *Sa* and *Sq*, with the NiP2 that improved the RR performance of 21% respect an identical retroreflector machined in a traditional mold steel.

When strictly comparing the quality of the facets produced by PBE with that generated through the proposed approach, the latter underperforms at *Sa* = 56 nm. However, it is noteworthy to mention that surface waviness yielded comparable values and that the proposed approach can be further improved, e.g. by using single-crystal diamond micromilling tools and coatings with higher phosphorous content. As regards operating costs, NiP micromilling results less expensive than Pin Bundling technology. In fact, considering the machining time (< 0.5 h) and the NiP coating cost (about 150€ for the whole mold insert), the proposed approach is suitable for being already implemented in the mold-maker industrial field.

Furthermore, the design freedom associated with micromilling of NiP-coated molds makes its development worthwhile to be further investigated for its ability to produce 3D freeform optical

microstructures (e.g. of significantly different sizes onto the same base substrate) and to largely reduce manufacturing time and cost.

References

[1] Nilsen, R.B., Lu, X.J., Retroreflection technology (2004) *Opt. Photonics Counterterrorism Crime Fighting*, 5616:47-60.

[2] Hussein, S., Hamilton, B., Tutunea-Fatan, O.R., Bordatchev, E.V. (2016) Novel retroreflective micro-optical structure for automotive lighting applications, *SAE Int. J. Passeng. Cars – Mech. Syst.*, 9:497-506.

[3] Sortino, M., Motyl, B., Totis, G. (2014) Preventive evaluation of mould production cost in aluminium casting, *Int J Adv Manuf Technol*, 70:285-295

[4] Milliken, N., Tutunea-Fatan, O.R., Bordatchev, E.V. (2019) Analysis of surface quality during fabrication of automotive retroreflectors, *Measurement*, 134:649-657.

[5] Bennett, H.E., Porteus, J.O. (1961) Relation between surface roughness and specular reflection at normal incidence, *J. Opt. Soc. Am. (JOSA)*, 51(2):123–9.

[6] Beich, W.S., Fendrock, L., Smock, C., Turner, N. (2008) Recent trends in precision polymer optics fabrication, *Proceeding of the Optical Fabrication and Testing, Optical Society of America*, p. OTuB5

[7] Sorgato, M., Masato, D., Lucchetta, G. (2017) Effect of vacuum venting and mold wettability on the replication of micro-structured surfaces, *Microsystem Technol.*, 23:2543-2552

[8] Milliken, N., Hamilton, B.W., Hussein, S., Tutunea-Fatan, O.R., Bordatchev, E.V. (2018) Enhanced bidirectional ultraprecise single point inverted cutting of right triangular prismatic retroreflectors, *Precision Engineering*, 52:158-169.

[9] Brinksmeier, E., Riemer, O., Gläbe, R. (2006) Merging technologies for optics, *Proc. of the 11th International Conference on Precision Engineering (ICPE), Tokyo, Japan*, pp. 1–9.

[10] Pramanik, A., Neo, K.S., Rahman, M., Li, X.P., Sawa, M., Maeda, Y. (2003) Cutting performance of diamond tools during ultra-precision turning of electroless-nickel plated die materials, *J. Mater. Process. Technol.*, 140:308-313.

[11] Yan, J., Oowada, T., Zhou, T., Kuriyagawa, T. (2009) Precision machining of microstructures on electroless-plated NiP surface for molding glass components, *J. Mater. Process. Technol.*, 209/10:4802-4808.

[12] Kobayashi, R., Xu, S., Shimada, K., Mizutani, M., Kuriyagawa, T., (2017) Defining the effects of cutting parameters on burr formation and minimization in ultra-precision grooving of amorphous alloy, *Precis. Eng.*, 49:115-121.

[13] Roeder, M., Drexler. M., Guenther, T., Zimmermann, A. (2018) Evaluation of ultra-precision milling strategies for micro lens array mould insert for the replication by injection-compression moulding, *Euspen's 18 International Conference.*

[14] Bonaiti, G., Parenti, P., Annoni, M., Kapoor, S. (2017) Micro-milling machinability of DED additive titanium Ti-6Al-4V, *45th SME North American Manufacturing Research Conference*

[15] Parenti, P., Masato, D., Sorgato, M., Lucchetta, G., Annoni, M. (2017) Surface Footprint in molds micromilling and effect on part demoldability in micro injection molding, *Journal of Manufacturing Processes*, 29:160-174

[16] Ning, J., Nguyen, V., Huang, Y., Hartwig, K.T., Liang, S.Y. (2019) Constitutive modeling of ultra-fine-grained titanium flow stress for machining temperature prediction, *Bio-Design and Manufacturing*

[17] Ning, J., Nguyen, V., Liang, S.Y. (2019) Analytical modeling of machining forces of ultra-fine-grained titanium, *The Int J Adv Manuf Technol*, 101:627-636

[18] Lucchetta, G., Fiorotto, M., Bariani, P.F. (2012) Influence of rapid mold temperature variation on surface topography replication and appearance of injection-molded parts, *CIRP Ann. Manuf. Technol.*, 61/1:539-542.

[19] Baruffi, F., Parenti, P., Cacciatore, F., Annoni, M., Tosello, G. (2017) On the application of replica molding technology for the indirect measurement of surface and geometry of micromilled components, *Micromachines*, 8(6),195

[20] ISO 25178 (2012) Geometrical product specification (GPS)—surface texture: areal

[21] ISO 4288 (1996) Geometrical product specification (GPS)—surface texture: profile method-rules and procedures for the assessment of surface texture. International Organization of Standardization

[22] Leach, R. (2013) Characterization of areal surface texture, *Springer, Heidelberg.*